RESEARCH PAPER

CrossMark

Simultaneous optimization of piezoelectric actuator topology and polarization

Juliano F. Gonçalves[1] · Daniel M. De Leon[2] · Eduardo A. Perondi[1]

Abstract

This article addresses the problem of piezoelectric actuator design for active structural vibration control. The topology optimization method using the Piezoelectric Material with Penalization and Polarization (PEMAP-P) model is employed in this work to find the optimum actuator layout and polarization profile simultaneously. A coupled finite element model of the structure is derived assuming a two-phase material, and this structural model is written into the state-space representation. The proposed optimization formulation aims to determine the distribution of piezoelectric material which maximizes the controllability for a given vibration mode. The optimization of the layout and poling direction of embedded in-plane piezoelectric actuators are carried out using a Sequential Linear Programming (SLP) algorithm. Numerical examples are presented considering the control of the bending vibration modes for a cantilever and a fixed beam. A Linear-Quadratic Regulator (LQR) is synthesized for each case of controlled structure in order to compare the influence of the polarization profile.

Keywords Topology optimization · PEMAP-P · Piezoelectric actuator · Controllability Gramian

1 Introduction

Piezoelectric materials are characterized by the capability of converting electrical energy into mechanical energy and vice-versa. This class of materials has been widely used in several engineering applications, as static shape control, micro electromechanical systems (MEMS) and energy harvesting devices (Irschik 2002; Priya 2007). In particular, the use of piezoelectric actuators (embedded or bonded) in host structures is usually considered effective for active vibration control.

Several aspects must be taken into account in order to achieve a desired control performance, including the actuator design and placement. The actuator design employing topology optimization method is a suitable procedure since it is considered a powerful tool when looking for performance improvements at the conceptual design stage.

For multi-material problems, some topology optimization approaches have been developed. For instance, Bendsøe and Sigmund (1999) proposed a mixture rule in the Solid Isotropic Material with Penalization (SIMP) method based on the material distribution concept. Yin and Ananthasuresh (2001) proposed an interpolation model for multi-phase materials considering a linear combination of normal distribution functions in a way that only one design variable is used for each element. However, this material model becomes highly nonlinear when more than two solid phases are involved. Recently, Zuo and Saitou (2017) presented a piece-wise interpolation model for the multi-material optimization without introducing any new variables.

✉ Juliano F. Gonçalves
   juliano.fagundes@ufrgs.br

   Daniel M. De Leon
   daniel.leon@ufrgs.br

   Eduardo A. Perondi
   perondi@mecanica.ufrgs.br

[1] Laboratory of Mechatronics and Control (LAMECC), Department of Mechanical Engineering, Federal University of Rio Grande do Sul, Sarmento Leite, 425, 90050-170, Porto Alegre, RS, Brazil

[2] Applied Mechanics Group (GMAp), Department of Mechanical Engineering, Federal University of Rio Grande do Sul, Sarmento Leite, 425, 90050-170, Porto Alegre, RS, Brazil

Piezoelectric and dielectric properties also need to be interpolated for problems in which one phase is a piezoelectric material. Silva and Kikuchi (1999) proposed the Piezoelectric Material with Penalization (PEMAP) model, which is an extension of the SIMP model where the power law is also used to interpolate these properties. This approach has been extensively used to design piezoelectric transducers. Carbonari et al. (2007) formulated a simultaneous topology optimization problem for the host structure, piezoceramic domain and piezoceramic rotation angles considering both the maximization of output displacements or forces. Wein et al. (2009) dealt with the topology optimization problem of piezoelectric actuator patches aiming to maximize the resonance response under harmonic excitation. Silveira et al. (2015) and Gonçalves et al. (2016) studied the actuator topology design using controllability measures. They predefined the electrode configuration imposing null-polarity phases separating areas of different independent electrodes in order to avoid short-circuiting. However, this null-polarity domain is arbitrarily chosen and, therefore, can lead to poor quality solutions. Kang et al. (2011) included a new design variable to represent the spatial distribution of the control voltage. By some means, this work is connected with the electrodes polarity problem.

Based on the PEMAP model, Kögl and Silva (2005) introduced another design variable for the piezoelectric polarization of the material. This is the so-called PEMAP-P (Piezoelectric Material with Penalization and Polarization) model. Nakasone and Silva (2010) combined the PEMAP-P model with the Rational Approximation of Material Properties (RAMP) (Stolpe and Svanberg 2001) to reduce numerical instabilities as gray scale appearance and localized modes in dynamic problems. Luo et al. (2010) studied the topology optimization of a multi-phase compliant actuator considering the design of both host structure and piezoelectric parts. Kiyono et al. (2012) combined the PEMAP-P model with the Discrete Material Optimization (DMO) (Lund 2009) approach to consider also the fiber orientation for the design of laminated piezocomposite shell transducers. The polarization profile optimization was studied by Donoso and Bellido (2009) considering a fixed host structure and, recently, along with the host structure optimization (Ruiz et al. 2016) for the piezoelectric transducers design.

In this paper, the design of embedded in-plane piezoelectric actuators is carried out by means of an optimization procedure using the controllability Gramian. The literature review reveals that, to the best of authors knowledge, there seems to be no contributions on the controllability-based topology optimization of piezoelectric actuators considering its layout and poling direction simultaneously. Therefore, the concept of topology optimization, based on the PEMAP-P model, is employed in this work to find both the layout and polarization profile of piezoelectric actuators which maximizes the control performance for a target vibration mode. The topology optimization problem is solved using a Sequential Linear Programming (SLP) algorithm. Numerical examples are presented considering the application of a Linear Quadratic Regulator (LQR) scheme. The control is synthesized for the piezoelectric actuators with both uniform and optimal polarization profiles and their dynamic responses are compared in order to verify the performance improvement.

2 Structural modeling

In this work, the goal is to design piezoelectric actuators in the most suitable way to suppress the vibration of a single target mode, considering a set of actuators embedded in a structure with fixed domain boundary. Figure 1a shows the general problem for topology optimized actuator design. The physical domain, $\Omega = \Omega_b \cup \Omega_d$, is split into two parts: a base domain, Ω_b, and a design domain, Ω_d. The base domain plays only structural role while the design domain is also responsible for the actuation. As mentioned above, the design domain is also split into two parts: a positive-polarized piezoelectric domain, Ω_p, and a negative-polarized piezoelectric domain, Ω_n. The domain boundary, $\Gamma = \Gamma_d \cup \Gamma_n$, is composed of two parts: the Dirichlet boundary with prescribed displacements, Γ_d, and the Neumann boundary with zero normal stress, Γ_n.

The body has its upper and lower surfaces covered with thin electrodes, which are subjected to prescribed voltages, as represented in Fig. 1b where P and E are the poling and electric field directions. Therefore, it is possible to produce both tensile and compressive fields in different regions of the body using the same control voltage and pair of electrodes.

2.1 Constitutive equations for a three-phase material

A standard committee of the IEEE published a well-known description of a piezoelectric media behavior, which consists of two linear constitutive relations (Meitzler et al. 1988):

$$T_i = c_{ij}S_j - d_{ki}E_k \tag{1}$$

$$D_i = d_{ij}S_j + e_{ik}E_k \tag{2}$$

where E_k denotes the electric field vector, T_i is the mechanical stress vector, S_j is the mechanical strain vector, and D_i is the electric displacement vector. Moreover, c_{ij}, d_{ij} and e_{ij} are the elastic, piezoelectric coupling and dielectric
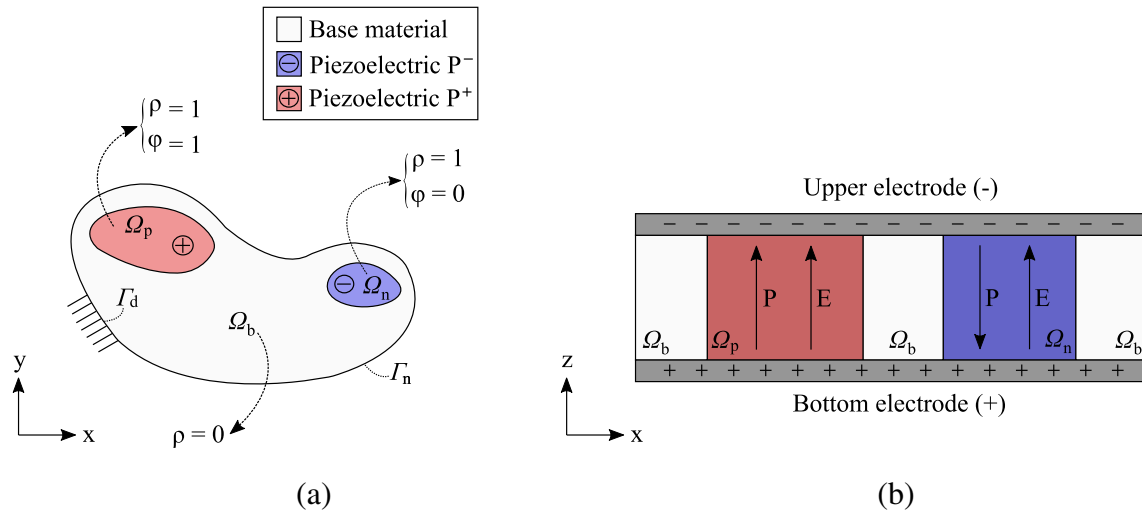
Fig. 1 General problem for topology optimized actuator design: **a** boundary conditions and **b** electrode configuration

constants, respectively. These constitutive equations consider linear behavior, which is acceptable when low stresses and electric intensity fields are applied. Otherwise, piezoelectric ceramics can present nonlinear behavior, especially hysteretic effects (Chen and Montgomery 1980).

A linear interpolation is used to describe the constitutive constants within the physical domain. Therefore, one can consider the same linear constitutive relations for both base domain, Ω_b, and design domain, Ω_d. Thus, one can respectively define elastic, piezoelectric and dielectric properties by means of:

$$c_{ij} = \rho c_{ij}^{pzt} + (1 - \rho)c_{ij}^{base} \qquad (3)$$

$$d_{ij} = \rho(2\varphi - 1)d_{ij}^{pzt} \qquad (4)$$

$$e_{ij} = \rho(2\varphi - 1)e_{ij}^{pzt} \qquad (5)$$

Similarly, the interpolated material density can be written as:

$$\gamma = \rho\gamma^{pzt} + (1 - \rho)\gamma^{base} \qquad (6)$$

where ρ and φ are variables which define the presence of piezoelectric material and its poling direction; c_{ij}^{base} and c_{ij}^{pzt} are the elastic properties of base and piezoelectric material; d_{ij}^{pzt} and e_{ij}^{pzt} are the electromechanical coupling and dielectric properties of the piezoelectric material; γ^{base} and γ^{pzt} are the density of base and piezoelectric material, respectively. According to this material model, a given point within the physical domain is defined as active piezoelectric material with positive polarization if $\rho = 1$ and $\varphi = 1$, while negative polarization is defined if $\rho = 1$ and $\varphi = 0$. Consequently, a passive base material is defined if $\rho = 0$, as represented in Fig. 1a.

2.2 Finite element model and modal analysis

The Hamilton's variational principle extended to a piezoelectric media (Lerch 1990) is an equivalent description of the boundary value problem. Assuming proper finite element approximations (Allik and Hughes 1970), the global equations which govern the spatial movement for a discretized body are written as:

$$\mathbf{M}_{uu}\ddot{\mathbf{u}} + \mathbf{C}_{uu}\dot{\mathbf{u}} + \mathbf{K}_{uu}\mathbf{u} + \mathbf{K}_{u\phi}\boldsymbol{\phi} = \mathbf{0} \qquad (7)$$

where $\mathbf{u}$ is the displacement vector, $\boldsymbol{\phi}$ is the voltage vector, $\mathbf{M}_{uu}$ is the mass matrix, $\mathbf{C}_{uu}$ is the damping matrix, $\mathbf{K}_{uu}$ is the stiffness matrix, $\mathbf{K}_{u\phi}$ is the piezoelectric coupling matrix and the upper dot denotes time derivative.

The piezoelectric patch can be configured in either open- or short-circuit, depending on whether the bottom and upper electrodes are connected. This first type, also called as sensor configuration, occurs when both electrodes are disconnected and the voltage depends on the structural dynamics (Becker et al. 2006). For the short-circuit configuration, it is assumed that both electrodes are grounded and, therefore, the generalized eigenvalue problem is written as:

$$\mathbf{K}_{uu}\boldsymbol{\psi} = \omega^2\mathbf{M}_{uu}\boldsymbol{\psi} \qquad (8)$$

where $\boldsymbol{\psi}$ and ω are the eigenvector and the eigenfrequency, respectively.

The structural model can be truncated to consider only a few representative modes for the global dynamic response. Therefore, the displacement vector $\mathbf{u}$ is approximated by:

$$\mathbf{u} \approx \boldsymbol{\Psi}\boldsymbol{\eta} = \sum_{i\in\mathbb{M}} \boldsymbol{\psi}_i\eta_i \qquad (9)$$

where $\boldsymbol{\Psi}$ is the truncated modal matrix, $\boldsymbol{\eta}$ is the corresponding vector of modal coordinates, and $\mathbb{M}$ is a set

containing the representative modes. Using this approximation, one can rewrite (7) into the reduced modal space as:

$$\ddot{\boldsymbol{\eta}} + \boldsymbol{\Lambda}\dot{\boldsymbol{\eta}} + \boldsymbol{\Omega}^2\boldsymbol{\eta} + \boldsymbol{\Psi}^{\mathrm{T}}\mathbf{K}_{u\phi}\boldsymbol{\phi} = \mathbf{0} \tag{10}$$

where $\boldsymbol{\Omega}$ is the diagonal matrix of natural frequencies, and:

$$\boldsymbol{\Lambda} = \underset{i \in \mathbb{M}}{\mathrm{diag}}\,(2\zeta_i\omega_i) \tag{11}$$

is the modal damping matrix in which ζ_i and ω_i are the natural modal damping ratio and frequency of the i-th mode, respectively. The damping matrix is usually unknown when dealing with continuous problems. Therefore, the definition of a model in the modal coordinates stablishes an important advantage since damping properties are conveniently evaluated in terms of these coordinates (Gawronski 2004).

3 Actuator topology design using the controllability Gramian

3.1 Controllability of a dynamic system

Since the electrical degrees of freedom $\boldsymbol{\phi}$ are the actuator control voltage, the term $\boldsymbol{\Psi}^{\mathrm{T}}\mathbf{K}_{u\phi}\boldsymbol{\phi}$ in (10) can be considered as an external force. Consequently, the equation of motion can be stated in the state-space representation as the following system of constant coefficient linear differential equations:

$$\dot{\mathbf{x}} = \mathbf{A}\mathbf{x} + \mathbf{B}\boldsymbol{\phi} \tag{12}$$

where $\mathbf{x}$ is the state vector, $\mathbf{A}$ is the system matrix and $\mathbf{B}$ is the control input matrix. In this work, the state variables are defined as the truncated modal displacements and velocities, $\mathbf{x} = \{\boldsymbol{\eta} \quad \dot{\boldsymbol{\eta}}\}^{\mathrm{T}}$ which is a straightforward approach and present direct physical interpretation (Gawronski 2004). Thus, the system and control input matrices are respectively given by:

$$\mathbf{A} = \begin{bmatrix} \mathbf{0} & \mathbf{I} \\ -\boldsymbol{\Omega}^2 & -\boldsymbol{\Lambda} \end{bmatrix} \tag{13}$$

$$\mathbf{B} = \begin{bmatrix} \mathbf{0} \\ -\boldsymbol{\Psi}^{\mathrm{T}}\mathbf{K}_{u\phi} \end{bmatrix} \tag{14}$$

where $\mathbf{I}$ and $\mathbf{0}$ are the appropriately dimensioned identity and zero matrices, respectively.

The system controllability will depend on the structural dynamics (matrix $\mathbf{A}$) and actuator design parameters, which are included in matrix $\mathbf{B}$. A structure is considered controllable if the actuators are able to excite the structural modes of interest. One way to determine such feature is using the so-called controllability Gramian ($\mathbf{W}$) (Preumont 2011). It is defined as:

$$\mathbf{W}(\tau) = \int_0^\tau e^{\mathbf{A}t}\mathbf{B}\mathbf{B}^{\mathrm{T}}e^{\mathbf{A}^{\mathrm{T}}t}\,dt \tag{15}$$

When dealing with stable systems, we can consider the stationary solutions, i.e., $\dot{\mathbf{W}} = \mathbf{0}$, which allows obtaining the controllability Gramian by the Lyapunov equation (Gawronski 2004):

$$\mathbf{A}\mathbf{W} + \mathbf{W}\mathbf{A}^{\mathrm{T}} = -\mathbf{B}\mathbf{B}^{\mathrm{T}} \tag{16}$$

where $\mathbf{W} = \mathbf{W}(\infty)$. The system is controllable, i.e, all states $\mathbf{x}$ can be excited by the control input $\boldsymbol{\phi}$, if and only if $\mathbf{W}$ is positive definite (Gawronski 2004; Preumont 2011). The Gramian evaluation requires the numerical solution of a Lyapunov equation, which is obtained using, for instance, the Bartels-Stewart (B-S) method (Bartels and Stewart 1972) or the Hammarling's method (Hammarling 1991). The latter is an alternative to the B-S method when the Lyapunov equation is stable and its right-hand side is semidefinite (Penzl 1998).

3.2 Topology optimization formulation

In most cases, two types of perturbation can excite a flexible structure: transient or persistent. For a transient perturbation, the control system aims to lead the dynamic system to a desired space in a given time interval with the minimum control effort. When dealing with persistent perturbation, the energy transmitted from the actuators to the structure should be maximized in order to minimize the perturbation effects. Hać and Liu (1993) derived controllability indexes to help finding the optimum actuators placement considering both transient and persistent problems. However, both approaches can be used in actuator placement problems for structures with small damping ratios and well-spaced frequencies (Hać and Liu 1993; Leleu et al. 2000). Considering an initial condition given by $\mathbf{x}(0) = \mathbf{x}_0$, the optimum actuator placement is the one which expend less energy to lead the dynamic system to a desired space $\mathbf{x}(\tau) = \mathbf{x}_\tau$ after a time interval τ. Thus, one can write the following minimum energy problem (Middleton and Goodwin 1990):

$$\begin{aligned} \min : \quad & \mathcal{F} = \int_0^\tau \boldsymbol{\phi}^{\mathrm{T}}(t)\boldsymbol{\phi}(t)\,dt \\ \text{s.t.} : \quad & \mathbf{x}(0) = \mathbf{x}_0 \\ : \quad & \mathbf{x}(\tau) = \mathbf{x}_\tau \\ : \quad & \dot{\mathbf{x}}(t) = \mathbf{A}\mathbf{x}(t) + \mathbf{B}\boldsymbol{\phi}(t) \end{aligned} \tag{17}$$

This problem has a known solution, which can be written in terms of the controllability Gramian (Hać and Liu 1993) and the minimal energy:

$$\mathcal{F}_{min} = \left(e^{\mathbf{A}\tau}\mathbf{x}_0 - \mathbf{x}_\tau\right)^{\mathrm{T}}\mathbf{W}^{-1}(\tau)\left(e^{\mathbf{A}\tau}\mathbf{x}_0 - \mathbf{x}_\tau\right) \tag{18}$$

Then, the minimal energy required to lead the system from $\mathbf{x}_0$ to $\mathbf{x}_\tau$ in a time interval τ is obtained if a norm of $\mathbf{W}^{-1}(\tau)$ is minimized.

Considering the time integral form in (15), the steady state solution for the controllability Gramian can be stated as:

$$\mathbf{W}(\infty) = \mathbf{W}(\tau) + \int_{\tau}^{\infty} e^{\mathbf{A}t} \mathbf{B}\mathbf{B}^{\mathrm{T}} e^{\mathbf{A}^{\mathrm{T}}t} \, dt \qquad (19)$$

This equation can be rewritten as (Hać and Liu 1993):

$$\mathbf{W}(\tau) = \mathbf{W}(\infty) - e^{\mathbf{A}\tau} \mathbf{W}(\infty) e^{\mathbf{A}^{\mathrm{T}}\tau} \qquad (20)$$

where $e^{\mathbf{A}\tau}$ depends only on the structure dynamics and the time interval τ. Moreover, $\| e^{\mathbf{A}\tau} \| \to 0$ when $T \to \infty$ for a stable system. Therefore, the optimum actuator placement is the one that maximizes some norm of $\mathbf{W}(\infty)$ (Hać and Liu 1993).

Following the above-mentioned premise, the proposed topology optimization formulation aims to maximize the controllability for a given vibration mode. This formulation is written in terms of the eigenvalues of $\mathbf{W}$ which are proportional to the energy transmitted from the actuator to the structure for individual vibration modes (Hać and Liu 1993). Therefore, this controllability measure is suitable for both transient and persistent perturbations. The optimization problem is written as:

$$\begin{aligned} \max_{\boldsymbol{\rho}, \boldsymbol{\varphi}} : \quad & f = \lambda_k \\ \text{s.t.} : \quad & g_1 = \frac{\sum_{i \in \mathbb{N}} \rho_i}{V} \le C_V \\ & 0 \le \rho_i \le 1 \quad i \in \mathbb{N} \\ & 0 \le \varphi_i \le 1 \quad i \in \mathbb{N} \end{aligned} \qquad (21)$$

where ρ_i and φ_i are the design variables associated with the i-th element, λ_k is the eigenvalue related to the k-th vibration mode, V is the volume of the physical domain, C_V is a threshold for the piezoelectric material volume and $\mathbb{N}$ is the set containing all elements. It is important to remark that this formulation is valid for structures with small damping ratios. Otherwise, the relationship between eigenvalues λ_i and energy for individual vibration modes is not directly found. The controllability Gramian eigenvalues are positive real numbers (since $\mathbf{W}$ is assumed to be positive-definite throughout the optimization process) obtained by solving the following problem:

$$(\mathbf{W} - \lambda_i \mathbf{I}) \boldsymbol{\sigma}_i = \mathbf{0} \qquad (22)$$

with

$$\boldsymbol{\sigma}_i^{\mathrm{T}} \boldsymbol{\sigma}_i = 1 \qquad i \in \mathbb{S} \qquad (23)$$

where λ_i is the i-th eigenvalue of $\mathbf{W}$, $\boldsymbol{\sigma}_i$ is its respective eigenvector, and $\mathbb{S}$ is the set containing all states. This formulation considers truncated modal space $\mathbb{M}$ to represent the dynamic behavior of a flexible structure. Spillover instabilities can occur when a truncated model is used to synthesize the controller for a continuous structure (Preumont 2011). However, we are not considering these undesirable effects in this formulation. A limit to the control

spillover, which refers to the control input exciting vibration modes that are not included in the truncated model, was investigated by Gonçalves et al. (2017).

The optimization problem proposed here can be described as the optimum layout material of three phases with non-vanishing stiffness. These phases are defined according to the discrete element-wise design variables $\boldsymbol{\rho}$ and $\boldsymbol{\varphi}$. This type of problem is an integer optimization, i.e., the design variables can assume only values 0 or 1. However, integer optimization of the continuous problem is ill posed, and its spatial discretization might not converge with the mesh refinement, i.e., one can find different topologies for different mesh sizes, thus a unique solution is nonexistent. Therefore, a relaxed continuous optimization is formulated by introducing a constitutive parameterization which allows the design variables to assume intermediate values in the interval $\rho_{min} \le \rho_i \le 1$ and $0 \le \varphi_i \le 1$, where the subscript refers to the i-th design variable and ρ_{min} is a small lower bound, commonly imposed to avoid singularity issues when solving the equilibrium problem through FEM (Bendsøe and Kikuchi 1988; Bendsøe et al. 2004). For this particular problem, the lower bound for the design variables $\boldsymbol{\rho}$ is set in order to avoid singularity problem when calculating the controllability Gramian $\mathbf{W}$, since this process requires the knowledge of input matrix $\mathbf{B}$ that depends on the piezoelectric coupling matrix which would be singular for ρ_i equals to zero.

Although this relaxed version of the optimization problem is efficient for many applications, it can present a solution with a large number of intermediate design variables, which is usually undesirable during the interpretation of the optimal distribution of material. A well-known method to force the solution to be as discrete as possible is the so-called SIMP (Solid Isotropic Material with Penalization) (Bendsøe and Sigmund 1999; Bendsøe et al. 2004).

Thus, the design variables are penalized as ρ_i^p in order to push intermediate values toward either 0 or 1. The local stiffness for $\rho_i < 1$ is lowered by specifying an exponent value $p > 1$. Hence, there is an additional cost to have intermediate design variables in the final solution. Therefore, the design parameterization written in terms of the SIMP model can be expressed as (Bendsøe and Sigmund 1999):

$$c_{ij} = \rho^p c_{ij}^{pzt} + (1 - \rho^p) c_{ij}^{base} \qquad (24)$$

An extension of this approach is the Piezoelectric Material with Penalization and Polarization (PEMAP-P) proposed by Kögl and Silva (2005). Thus, the coupling piezoelectric and dielectric properties are written as:

$$d_{ij} = \rho^{p1} (2\varphi - 1)^{p2} d_{ij}^{pzt} \qquad (25)$$

$$e_{ij} = \rho^{p1} (2\varphi - 1)^{p3} e_{ij}^{pzt} \qquad (26)$$

where $p1$, $p2$ and $p3$ are penalization factors.

3.3 Sensitivity analysis

First-order optimization algorithms, as the Sequential Linear Programming (SLP), require the sensitivities of the objective function and constraints. Since the sensitivities with respect to both design variables are similar, we denote v as a variable that represents either ρ_i or φ_i.

3.3.1 Controllability Gramian sensitivity

Considering the problem presented in (22), eigenvalue derivatives with respect to v can be obtained by solving a new eigenanalysis problem for $\partial \lambda_j / \partial v$ (Wu et al. 2007):

$$\left[\boldsymbol{\sigma}_j^T \left(\frac{\partial \mathbf{W}}{\partial v} \right) \boldsymbol{\sigma}_j - \frac{\partial \lambda_j}{\partial v} \right] \boldsymbol{\gamma}_j = \mathbf{0} \tag{27}$$

where $\boldsymbol{\gamma}_j$ is the j-th eigenvector of the derivative eigenproblem. The sensitivity of the controllability Gramian is given by the differentiation of (16) with respect to the design variable v and, therefore, can be obtained by solving a new Lyapunov equation for $\partial \mathbf{W} / \partial v$:

$$\mathbf{A} \frac{\partial \mathbf{W}}{\partial v} + \frac{\partial \mathbf{W}}{\partial v} \mathbf{A}^T = -\mathbf{Q}_d \tag{28}$$

where

$$\mathbf{Q}_d = \left(\frac{\partial \mathbf{A}}{\partial v} \mathbf{W} + \mathbf{W} \frac{\partial \mathbf{A}^T}{\partial v} + \frac{\partial \mathbf{B}}{\partial v} \mathbf{B}^T + \mathbf{B} \frac{\partial \mathbf{B}^T}{\partial v} \right) \tag{29}$$

is a matrix which its components are known before solving each linear programming problem. Sensitivities of system and control input matrices are respectively given by:

$$\frac{\partial \mathbf{A}}{\partial v} = \begin{bmatrix} \mathbf{0} & \mathbf{0} \\ -\frac{\partial \mathbf{\Omega}^2}{\partial v} & -\frac{\partial \mathbf{\Lambda}}{\partial v} \end{bmatrix} \tag{30}$$

$$\frac{\partial \mathbf{B}}{\partial v} = \begin{bmatrix} \mathbf{0} \\ -\frac{\partial \mathbf{\Psi}^T}{\partial v} \mathbf{K}_{u\phi} - \mathbf{\Psi}^T \frac{\partial \mathbf{K}_{u\phi}}{\partial v} \end{bmatrix} \tag{31}$$

3.3.2 Eigenvalues and eigenvectors sensitivity

The sensitivities of the modal matrix and natural frequencies are evaluated following the method proposed by Wu et al. (2007) in which the occurrence of repeated eigenvalues is taken into account. If the solution of (8) has r repeated eigenvalues ω_j^2 for $j = 1, \ldots, r$, one can define a matrix with their respective eigenvectors $\mathbf{\Psi}_{re} = \left[\boldsymbol{\psi}_1, \ldots, \boldsymbol{\psi}_r \right]$ and, therefore, the sensitivity of the natural frequency is given by:

$$\left[\mathbf{\Psi}_{re}^T \left(\frac{\partial \mathbf{K}_{uu}}{\partial v} - \omega_j^2 \frac{\partial \mathbf{M}_{uu}}{\partial v} \right) \mathbf{\Psi}_{re} - \frac{\partial \omega_j^2}{\partial v} \mathbf{I} \right] \boldsymbol{\gamma}_j = \mathbf{0} \tag{32}$$

Unique eigenvalues $\mathbf{H} = [\mathbf{h}_1, \ldots, \mathbf{h}_r]$ can be defined by means of the relationship $\mathbf{H} = \mathbf{\Psi}_{re} \left[\boldsymbol{\gamma}_1, \ldots, \boldsymbol{\gamma}_r \right]$, where $\boldsymbol{\gamma}_j$ are distinct eigenvectors obtained by (32). Denoting $\mathbf{F}_j =$

$\left(\mathbf{K}_{uu} - \omega_j^2 \mathbf{M}_{uu} \right)$, one can write the derivative of (8) with respect to the design variable v as:

$$\mathbf{F}_j \frac{\partial \boldsymbol{\psi}_j}{\partial v} = -\frac{\partial \mathbf{F}_j}{\partial v} \boldsymbol{\psi}_j \tag{33}$$

where

$$\frac{\partial \mathbf{F}_j}{\partial v} = \frac{\partial \mathbf{K}_{uu}}{\partial v} - \omega_j^2 \frac{\partial \mathbf{M}_{uu}}{\partial v} - \frac{\partial \omega_j^2}{\partial v} \mathbf{M}_{uu} \tag{34}$$

The sensitivity $\partial \mathbf{h}_j / \partial v$ is assumed to have the form $\partial \mathbf{h}_j / \partial v = \mathbf{z}_j + \mathbf{H} \mathbf{w}$, where $\mathbf{z}_j$ is a particular solution of (33) which satisfies $\mathbf{F}_j \mathbf{z}_j = -(\partial \mathbf{F}_j / \partial v) \mathbf{h}_j$ and $\mathbf{w}$ is given by (Wu et al. 2007):

$$\mathbf{w}_j = -\frac{1}{2} \mathbf{h}_j^T \left(\frac{\partial \mathbf{M}_{uu}}{\partial \rho_i} \mathbf{h}_i + 2 \mathbf{M}_{uu} \mathbf{z}_j \right) \tag{35}$$

The following extended system of equations was introduced by Wu et al. (2007) with unknowns $\mathbf{z}_j$ and μ_{ij}:

$$\begin{bmatrix} \mathbf{F}_j & \bar{\mathbf{M}}_1 & \ldots & \bar{\mathbf{M}}_r \\ \bar{\mathbf{M}}_1^T & \mathbf{0} & \ldots & \mathbf{0} \\ \vdots & \vdots & \ddots & \vdots \\ \bar{\mathbf{M}}_r^T & \mathbf{0} & \ldots & \mathbf{0} \end{bmatrix} \begin{Bmatrix} \mathbf{z}_j \\ \mu_{1j} \\ \vdots \\ \mu_{rj} \end{Bmatrix} = \begin{Bmatrix} -\frac{\partial \mathbf{F}_j}{\partial v} \mathbf{h}_j \\ 0 \\ \vdots \\ 0 \end{Bmatrix} \tag{36}$$

where $\bar{\mathbf{M}}_j = \mathbf{M}_{uu} \boldsymbol{\psi}_j$, $\mathbf{z}_j = \partial \boldsymbol{\psi}_j / \partial v$ is the eigenvector sensitivity with a solution vector $\left\{ \mathbf{z}_j \ \mu_{1j} \ \ldots \ \mu_{rj} \right\}^T = \left\{ \mathbf{z}_j \ 0 \ \ldots \ 0 \right\}^T$.

This sensitivity analysis presented suitable efficiency in previous studies and for the cases analyzed in this work. A general review of the sensitivity analysis of eigenvalues and eigenvectors can be found in Seyranian et al. (1994). For the specific application in the piezoelectric field problem, Ha and Cho (2006) proposed a sensitivity analysis and topology optimization where repeated eigenvalues are also taken into account.

3.3.3 Material model sensitivity

The gradient of both mass and stiffness matrices are required to find the sensitivity of modal matrix and natural frequencies, which can be straightforward obtained. However, these terms depend on the material model. The gradients of the effective elastic properties and density are:

$$\frac{\partial c_{ij}}{\partial v} = \begin{cases} p\rho^{p-1} \left(c_{ij}^{pzt} - c_{ij}^{base} \right) & \text{if } v = \rho \\ 0 & \text{if } v = \varphi \end{cases} \tag{37}$$

$$\frac{\partial \gamma}{\partial v} = \begin{cases} \gamma^{pzt} - \gamma^{base} & \text{if } v = \rho \\ 0 & \text{if } v = \varphi \end{cases} \tag{38}$$

Finally, the gradient of the piezoelectric coupling properties is required to solve the term $\partial \mathbf{K}_{u\phi}/\partial v$ in (31):

$$\frac{\partial d_{ij}}{\partial v} = \begin{cases} p1\rho^{p1-1}(2\varphi-1)^{p2}d_{ij}^{pzt} & \text{if } v = \rho \\ 2\rho^{p1}p2(2\varphi-1)^{p2-1}d_{ij}^{pzt} & \text{if } v = \varphi \end{cases} \tag{39}$$

where all terms were already defined.

3.4 Optimization procedure

In this section, we discuss some numerical aspects of the optimization process. A flowchart of the implemented algorithm for solving the simultaneous problem is presented in Fig. 2 and some features of this algorithm are described.

The modal analysis is carried out applying a solid FE model using the formulation of an 8-node brick element with incompatible modes (Hughes 2012). For the initial s iterations, only the polarization design variables φ_i are calculated in order to avoid starting the simultaneous optimization with null-polarization elements.

The design variables are updated solving a linear programming (LP) problem which requires both objective and constraint functions to be linear. Otherwise, they can be
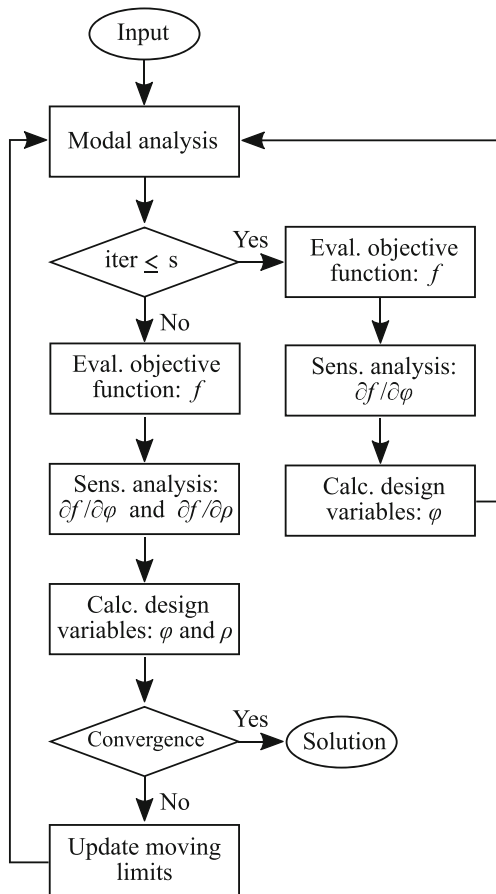

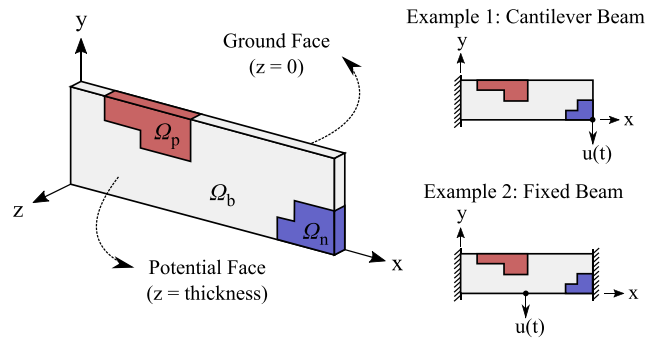**Fig. 2** Flowchart of analysis and optimization procedure

Fig. 3 Structure with embedded piezoelectric actuator and its boundary conditions

expressed by means of a Taylor series expansion truncated at the linear term. Then, side constraints should be included since this approximation is only acceptable for an arbitrary small neighborhood. These additional constraints, also called moving limits, are defined as

$$\rho_i^L \le \rho_i \le \rho_i^U, \quad i \in \mathbb{N} \tag{40}$$

$$\varphi_i^L \le \varphi_i \le \varphi_i^U, \quad i \in \mathbb{N} \tag{41}$$

where ρ_i^L and φ_i^L are the lower limits, and ρ_i^U and $\le \varphi_i^U$ are the upper limits. The update of the moving limits is carried out based on the design variables convergence.

The stopping criteria are based on the tolerance thresholds and take into account the values of design variables and objective function for the current (k) and previous iterations, as follows

$$\max\left\{\left|\left|\boldsymbol{\rho}^{(k)} - \boldsymbol{\rho}^{(k-1)}\right|\right|\right\} \le t_\rho \tag{42}$$

Table 1 Piezoelectric material properties (Rubio et al. 2009)

Elastic constant	$(10^{10}$ N/m$^2)$
c_{11}^{pzt}	12.10
c_{12}^{pzt}	7.54
c_{13}^{pzt}	7.52
c_{33}^{pzt}	11.10
c_{44}^{pzt}	2.11
c_{66}^{pzt}	2.26
Piezoelectric constant	(C/m^2)
d_{31}^{pzt}	-5.4
d_{33}^{pzt}	15.8
d_{51}^{pzt}	12.3
Dielectric constant	(F/m)
e_0	$8.85 \cdot 10^{-12}$
e_{11}^{pzt}/e_0	916
e_{33}^{pzt}/e_0	830
Density γ^{pzt}	7750 (kg/m^3)

$$\max\left\{\left|\left|\boldsymbol{\varphi}^{(k)} - \boldsymbol{\varphi}^{(k-1)}\right|\right|\right\} \leq t_{\varphi} \tag{43}$$

$$\left|\frac{f^{(k)}}{f^{(k-1)}} - 1\right| \leq t_f \tag{44}$$

where t_ρ and t_φ are tolerance thresholds for the design variables and t_f is the tolerance threshold for the objective function. The optimization solution is assumed as converged only if all stopping criteria have been simultaneously reached.

4 Numerical results and discussion

In this section, the proposed formulation is examined by means of two numerical examples: a cantilever beam and a fixed beam. The flexible structure with embedded in-plane piezoelectric actuator analyzed have two phases: passive base material Ω_b and active piezoelectric material $\Omega_d = \Omega_p \cup \Omega_n$, as presented in Fig. 3. The design domain Ω_d is
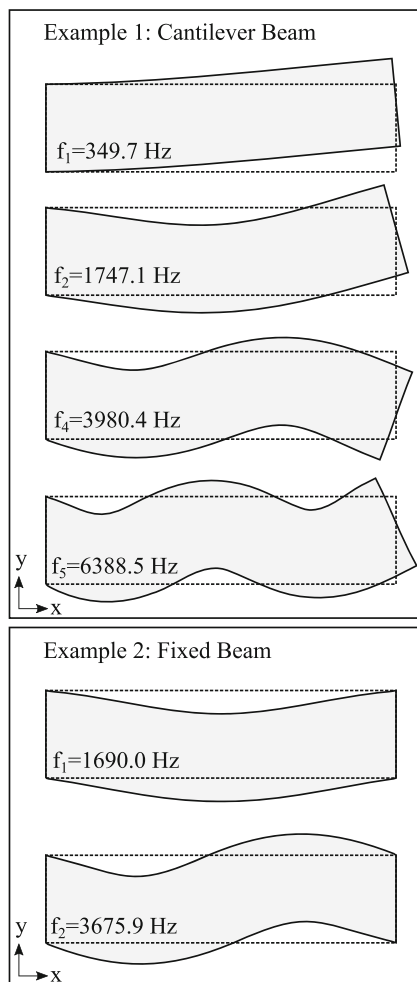

Fig. 4 Vibration modes considered in the optimization process

Example 1: Cantilever Beam

$f_1 = 349.7$ Hz

$f_2 = 1747.1$ Hz

$f_4 = 3980.4$ Hz

$f_5 = 6388.5$ Hz

Example 2: Fixed Beam

$f_1 = 1690.0$ Hz

$f_2 = 3675.9$ Hz

Table 2 Parameters used in the numerical simulations

Geometric parameter	(m)
Length	0.600
Height	0.150
Thickness	0.020
Number of elements	2400
Topology optimization parameter	
C_V	0.120
p	3
$p1$	3
$p2$	1
$p3$	1
s	2
t_ρ	0.040
t_φ	0.040
t_f	0.020
Initial design variables	
ρ_i (for $i \in \mathbb{N}$)	0.505
φ_i (for $i \in \mathbb{N}$)	0.505

defined according to the solution of the design variables ρ_i for $i \in \mathbb{N}$. Within this domain, the piezoelectric material can have positive or negative polarization direction, which depends on the design variables φ_i for $i \in \mathbb{N}$.

The passive base material phase is defined as an isotropic elastic material with aluminum constitutive properties ($E = 71 \cdot 10^9$ N/m^2, $\nu = 0.33$, and $\gamma = 2700$ kg/m^3). A piezoelectric ceramic PZT-5A is considered as the active material phase and its elastic, piezoelectric and dielectric constants are presented in Table 1.

The face with coordinates $z = 0$ is grounded and the input voltage is prescribed on the potential face, with $z = $ thickness, as represented in Fig. 3. Four vibration modes

Table 3 Description of the analyzed cases

| Case	Design variables	Example	Obj. function
A	ρ	Cant. Beam	λ_1
B	φ, ρ		
C	ρ	Cant. Beam	λ_2
D	φ, ρ		
E	ρ	Cant. Beam	λ_4
F	φ, ρ		
G	ρ	Cant. Beam	λ_5
H	φ, ρ		
I	ρ	Fixed Beam	λ_1
J	φ, ρ		
K	ρ	Fixed Beam	λ_2
L	φ, ρ		

Fig. 5 Optimal polarization φ, piezoelectric material distribution ρ and actuator design for: **a** case A and **b** case B
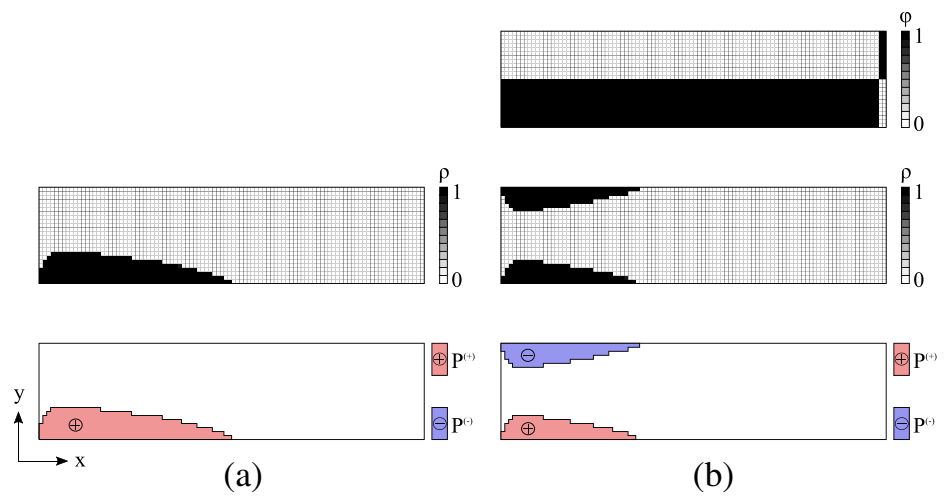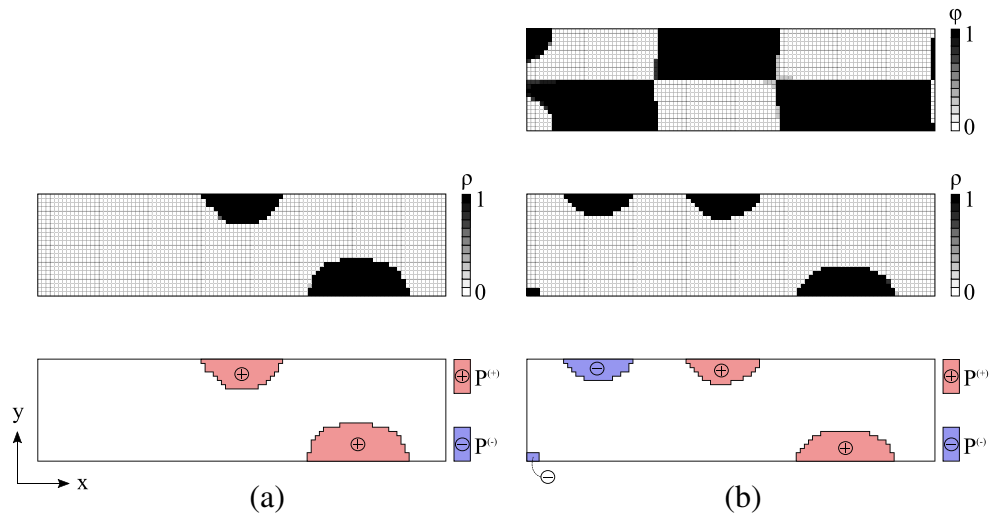

Fig. 6 Optimal polarization φ, piezoelectric material distribution ρ and actuator design for: **a** case C and **b** case D
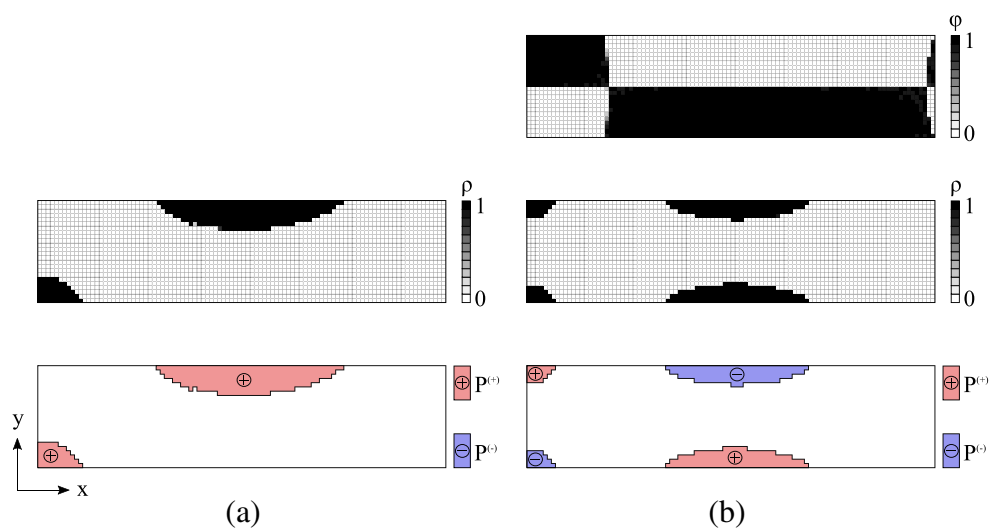
Fig. 7 Optimal polarization φ, piezoelectric material distribution ρ and actuator design for: **a** case E and **b** case F
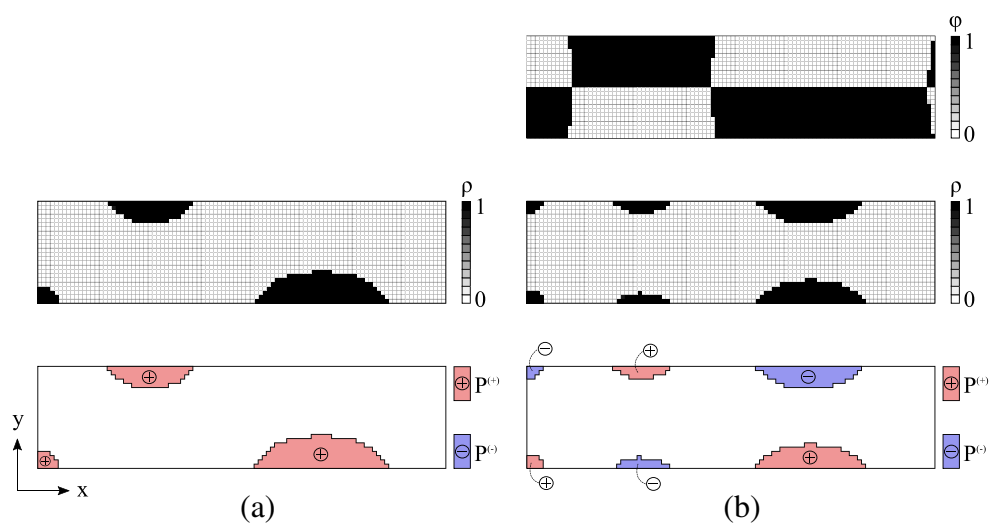
Fig. 8 Optimal polarization φ, piezoelectric material distribution ρ and actuator design for: **a** case G and **b** case H

for the cantilever beam example and two vibration modes for the fixed beam example, with the lower frequencies, are considered in the optimization procedure. These modes and their respective natural frequencies are presented in Fig. 4. We do not consider the third vibration mode (with natural frequency f_3) for the cantilever beam example since it is an extensional mode and the solution for the optimal polarization profile, when considering this mode, is a uniform distribution. Table 2 furnishes an overview of the main parameters used for the finite element mesh and topology optimization procedure.

The initial design variables φ_i for $i \in \mathbb{N}$ are set close to 0.500 in order to define elements with either positive or negative polarization from the first iterations.
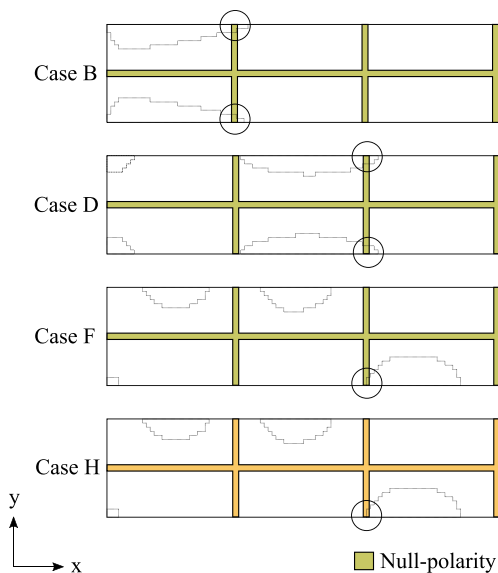
Fig. 9 Independent electrode configuration used in Silveira et al. (2015) along with the actuators designs obtained by the proposed formulation

Ill-conditioning problem occurs when $\varphi_i = 0.500$, then the variable is assumed to be either 0.495 or 0.505 when necessary. Tolerance parameters t_ρ, t_φ and t_f were set based on preliminary works solving the controllability problem. Several values for stopping the optimization problem were tested and the only difference observed was the time for convergence and no gain was obtained in the objective function for tighter values. Besides that, the interpretation of the final designs did not change the objective function value, which confirms we found solutions with a small amount of design variables with intermediate values. A brief description of the analyzed cases is presented in Table 3. It is considered, for each target vibration mode, the fixed uniform polarization (only ρ_i is evaluated and $\varphi_i = 1$ for $i \in \mathbb{N}$) and the simultaneous optimization where both ρ_i and φ_i are evaluated.

It is important to mention that the controllability Gramian eigenvalues are sorted according to their respective state and, therefore, vibration mode. Thus, λ_1 is related to the first mode controllability and it is not necessarilly the smallest eigenvalue.

4.1 Actuator designs

The solutions for the topology optimization problem are presented in this section. Both design variables distributions φ and ρ are presented as well as a discrete solution, which is obtained by means of an interpretation of the intermediate design variables.

Figure 5 presents the solution for the maximization of the first vibration mode controllability for the cantilever beam example. A symmetric solution is obtained when solving the simultaneous optimization. This design is expected since the optimal actuator placement is closer to the clamped face. Thus, both tensile and compressive strain fields can be caused by the actuators.

Fig. 10 Optimal polarization φ, piezoelectric material distribution ρ and actuator design for: **a** case I and **b** case J
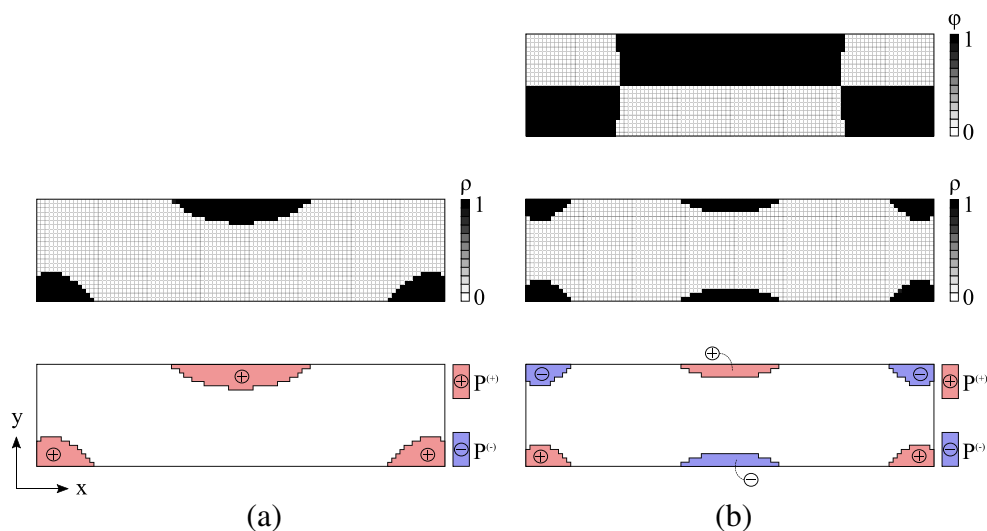
Figures 6 and 7 show the solution for the maximization of the controllability for the second and fourth vibration modes, respectively. Symmetric solutions also occur when solving the simultaneous optimization for these cases. This pattern does not occur for the last case, as can be observed in Fig. 8. However, the simultaneous optimization lead to a solution where piezoelectric material is also distributed in two regions close to the clamped face. These regions can be related to the nodal points of the beam neutral axis. Different starting points were tested for this case and the same final topology was obtained for this multi-start test. There is also no relationship between the non-symmetric solution and higher vibration modes since we have obtained symmetric solutions for higher modes of vibration. However, this type of problem is prone to show local minima and, therefore, it is important to mention that the proposed methodology cannot guarantee the global optimality.

For comparison purposes, Fig. 9 shows the actuators designs obtained by the proposed formulation and the

areas where the piezoelectric properties are neglected in order to separate the independent electrodes considered in Silveira et al. (2015). Circular markers highlight areas where the piezoelectric distribution would be restricted by this assumption. This comparison is very interesting, since it highlights the importance of not choosing null polarity regions a priori.

It is important to remark that we are not designing the electrode polarity profile. In that case, null-polarity areas should be imposed in order to avoid short-circuiting, as presented in Donoso and Sigmund (2016).

Figures 10 and 11 show the solution for the controllability maximization of the first and second vibration modes of the fixed beam, respectively. Symmetric solutions are also observed when solving the simultaneous optimization for these cases.

Figures 12 and 13 present the convergence histories for the analyzed cases. The most important feature of the formulation is that the simultaneous approach leads to higher

Fig. 11 Optimal polarization φ, piezoelectric material distribution ρ and actuator design for: **a** case K and **b** case L
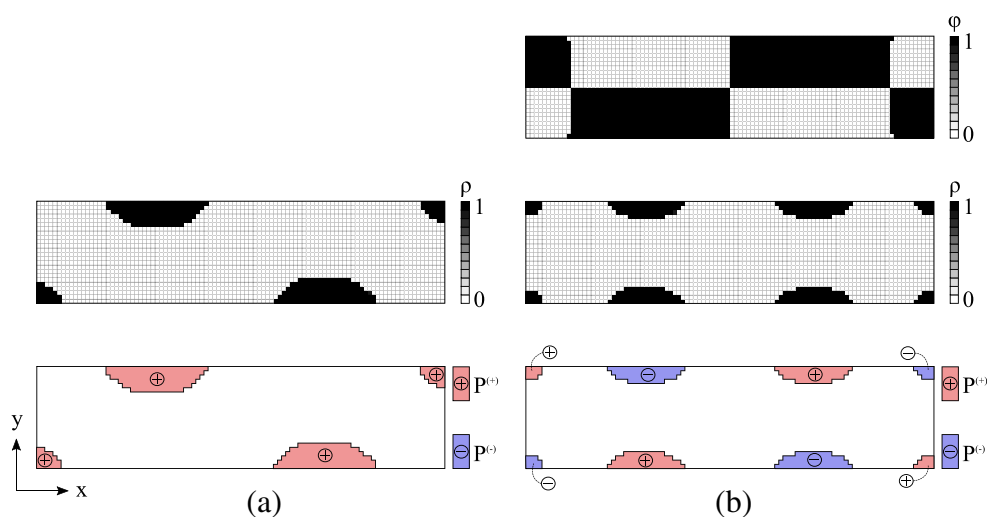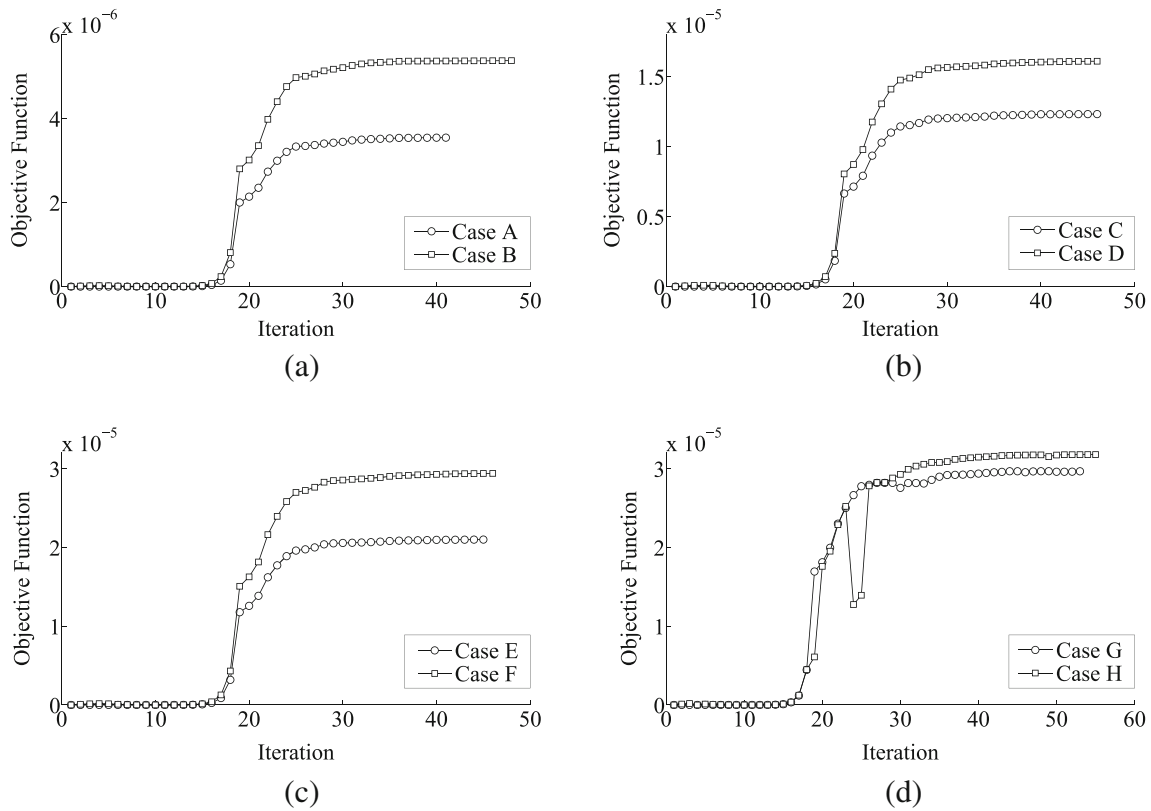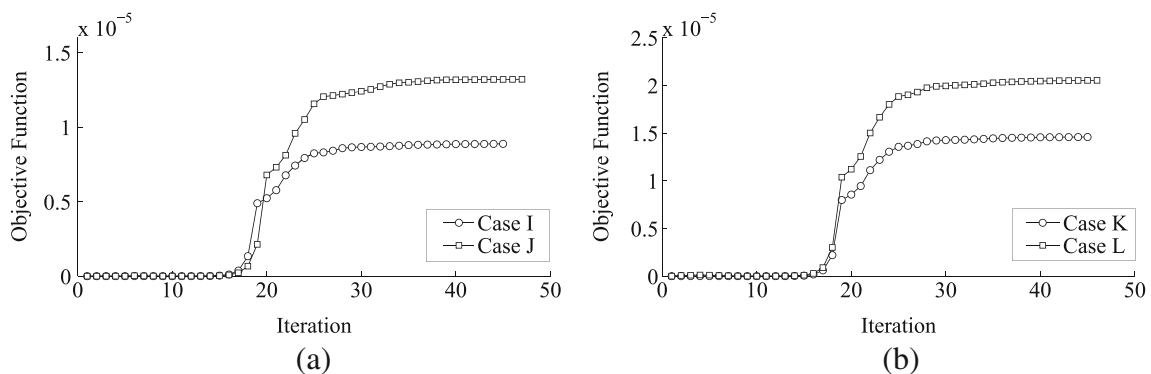
Fig. 12 Objective function convergence for the maximization of **a** λ_1, **b** λ_2, **c** λ_4 and **d** λ_5, considering the cantilever beam example

controllability measures. The only unusual behavior was observed in Case H, where a considerable jump occurs in the convergence history. This behavior is related to the update of the moving limits, which are relaxed according to the variables convergence. The solver is more susceptible to find either a non-feasible solution or a solution with no active constraint when the moving limits are relaxed. However, the solver presented sufficient robustness to find a feasible solution with active volume constraint right after this jumping point. Besides that, we can observe that the convergence is slow in the early steps of the optimization process

for all cases. This is explained by two main reasons. First, only the polarization variables (φ) are evaluated in the initial steps of the optimization process. These variables are less responsive than the distribution variables (ρ). Second, we start the optimization problem with $\rho_i = 0.505$, i.e, in the infeasible domain. Therefore, the algorithm spends some iterations to reach the feasible domain, delaying the convergence.

It is important to remark that the proposed formulation is prepared to take into account repeated eigenvalues in the sensitivity analysis. However, the examples studied in this

Fig. 13 Objective function convergence for the maximization of **a** λ_1 and **b** λ_2, considering the fixed beam example

Table 4 Free tip displacement and input voltage for the actuator designs obtained by the maximization of λ_1
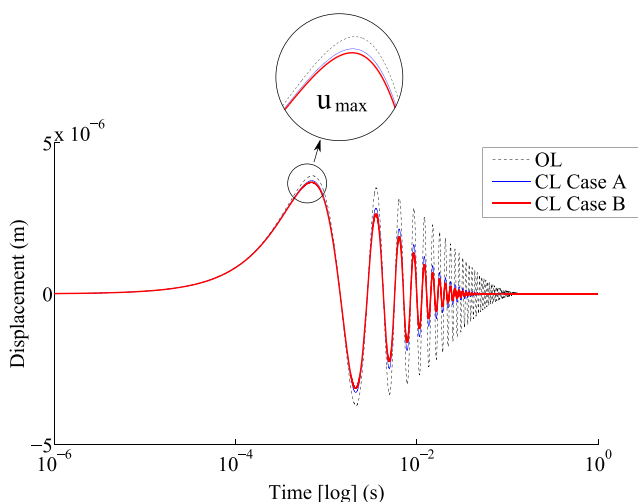
Case	q	u_{max} ($\times 10^{-6}$m)	u_{rms} ($\times 10^{-7}$m)	ϕ_{rms} (V)
A	1×10^{15}	3.749	2.034	4.859
B	1×10^{15}	3.695	1.851	4.773
A	1×10^{16}	3.285	1.173	11.850
B	1×10^{16}	3.139	1.049	10.958
A	1×10^{17}	2.282	0.610	23.541
B	1×10^{17}	2.061	0.530	21.360

Table 5 Free tip displacement and input voltage for the actuator designs obtained by the maximization of λ_2

Case	q	u_{max} ($\times 10^{-7}$m)	u_{rms} ($\times 10^{-8}$m)	ϕ_{rms} (V)
C	1×10^{15}	7.918	3.862	0.548
D	1×10^{15}	7.907	3.692	0.592
C	1×10^{16}	7.762	2.555	2.080
D	1×10^{16}	7.714	2.357	2.023
C	1×10^{17}	7.231	1.467	4.752
D	1×10^{17}	7.088	1.343	4.433

work are not prone to show this issue. In order to solve more complex problems where repeated eigenvalues and reversed modes are involved, it is also recommended the use of mode tracking schemes like, for instance, the Modal Assurance Criterion (MAC) (Kim and Kim 2000; Tsai and Cheng 2013).

4.2 Performance of the actuator designs

This work considered only the open-loop system, i.e., (12), on the optimization process. However, a state feedback control law is used to compare the performance of the actuator designs. This post-processing step is carried out employing a Linear-Quadratic Regulator (LQR) scheme in which the optimal feedback gain matrix is chosen to minimize a quadratic cost function subject to the system dynamics (Preumont 2011). The cost function is written as:

$$J = \frac{1}{2} \int_0^\tau (\mathbf{x}^T \mathbf{Q} \mathbf{x} + \phi^2 R)\, dt \tag{45}$$

Fig. 14 Free tip displacement response for the actuator designs obtained by the maximization of λ_1

where R is a positive weighting factor for the control input and $\mathbf{Q}$ is a semi-positive definite weighting matrix for the state variables:

$$\mathbf{Q} = \begin{bmatrix} q\mathbf{I} & \mathbf{0} \\ \mathbf{0} & \mathbf{I} \end{bmatrix} \tag{46}$$

where $\mathbf{I}$ and $\mathbf{0}$ are the appropriately dimensioned identity and zero matrices, respectively, and q is a weighting factor. Assuming full-state feedback, the gain matrix is

$$\mathbf{G} = R^{-1} \mathbf{B}^T \mathbf{P} \tag{47}$$

where $\mathbf{P}$ is the solution of the algebraic Riccati equation

$$\mathbf{A}^T \mathbf{P} + \mathbf{P}\mathbf{A} - R^{-1}\mathbf{P}\mathbf{B}\mathbf{B}^T\mathbf{P} + \mathbf{Q} = \mathbf{0} \tag{48}$$

Thus, the closed loop dynamics of the system becomes

$$\dot{\mathbf{x}} = (\mathbf{A} - \mathbf{B}\mathbf{G})\mathbf{x} \tag{49}$$

The displacement responses are evaluated considering an initial modal velocity. Figure 14 shows the displacement response due to the initial condition $\dot{\eta}_1(0) = 0.01$. Both open-loop (OL) and closed-loop (CL) are presented considering a controller with $q = 1 \times 10^{15}$. These displacement responses $u(t)$ are related to the vertical direction, and they are calculated for a point in the free end of the beam, as represented in Fig. 3.

Table 4 shows an overview of the results for the first mode control, in terms of the maximum displacement u_{max},

Table 6 Free tip displacement and input voltage for the actuator designs obtained by the maximization of λ_4

Case	q	u_{max} ($\times 10^{-7}$m)	u_{rms} ($\times 10^{-8}$m)	ϕ_{rms} (V)
E	1×10^{15}	3.502	1.596	0.169
F	1×10^{15}	3.500	1.545	0.191
E	1×10^{16}	3.478	1.153	0.817
F	1×10^{16}	3.469	1.064	0.815
E	1×10^{17}	3.383	0.679	2.091
F	1×10^{17}	3.354	0.618	1.955

Table 7 Free tip displacement and input voltage for the actuator designs obtained by the maximization of λ_5

Case	q	u_{max} ($\times 10^{-7}$m)	u_{rms} ($\times 10^{-8}$m)	ϕ_{rms} (V)
G	1×10^{15}	2.184	0.835	0.048
H	1×10^{15}	2.184	0.831	0.052
G	1×10^{16}	2.178	0.714	0.344
H	1×10^{16}	2.178	0.694	0.358
G	1×10^{17}	2.151	0.462	1.228
H	1×10^{17}	2.146	0.441	1.206

Table 9 Mid-length displacement and input voltage for the actuator designs obtained by the maximization of λ_2

Case	q	u_{max} ($\times 10^{-7}$m)	u_{rms} ($\times 10^{-8}$m)	ϕ_{rms} (V)
K	1×10^{15}	1.844	0.703	0.086
L	1×10^{15}	1.843	0.695	0.102
K	1×10^{16}	1.835	0.595	0.607
L	1×10^{16}	1.831	0.563	0.647
K	1×10^{17}	1.792	0.382	2.106
L	1×10^{17}	1.778	0.350	2.026

RMS displacement u_{rms}, and RMS control voltage ϕ_{rms}. The control energy required to lead the perturbed state to a desired rest state can be related to this voltage measure. For each case, three different values were assumed for the weighing factor q. One can observe that the displacements and RMS control voltage are lower when using the actuator designed by the simultaneous optimization procedure.

Results for the second mode control considering a response due to the initial condition $\dot{\eta}_2(0) = 0.01$ are presented in Table 5. For these cases, displacements and RMS control voltage are also lower when using the actuator designed by the simultaneous optimization excepting the control voltage when $q = 1 \times 10^{15}$.

Results for the control of the fourth and fifth vibration modes considering the response due to the initial conditions $\dot{\eta}_4(0) = 0.01$ and $\dot{\eta}_5(0) = 0.01$, respectively, are presented in Tables 6 and 7. Analogously, one can observe that the simultaneous approach leads to actuator designs with improved performance which can be observed especially when higher weighting factors q are used.

Results for the control of the first and second vibration modes for the fixed beam considering the response due to the initial conditions $\dot{\eta}_1(0) = 0.01$ and $\dot{\eta}_2(0) = 0.01$, respectively, are presented in Tables 8 and 9. These displacement responses $u(t)$ are related to the vertical direction, and they are calculated for a point in the mid-length of the fixed beam, as represented in Fig. 3.

Table 8 Mid-length displacement and input voltage for the actuator designs obtained by the maximization of λ_1

Case	q	u_{max} ($\times 10^{-7}$m)	u_{rms} ($\times 10^{-8}$m)	ϕ_{rms} (V)
I	1×10^{15}	3.945	1.459	0.191
J	1×10^{15}	3.942	1.438	0.226
I	1×10^{16}	3.896	1.215	1.297
J	1×10^{16}	3.875	1.142	1.377
I	1×10^{17}	3.665	0.768	4.336
J	1×10^{17}	3.590	0.699	4.144

Figures 15 and 16 present a comparison between the performance of actuator designs obtained using uniform and optimal polarization profiles. Difference in terms of RMS displacement $u_d = 1 - u^s_{rms}/u^u_{rms}$ and RMS control voltage $\phi_d = 1 - \phi^s_{rms}/\phi^u_{rms}$ are shown, where the superscript u refers to the cases with uniform polarization (A, C, E, G, I and K) and the superscript s refers to the cases with simultaneous optimization (B, D, F, H, J and L).

The piezoelectric actuator designed to control the first vibration mode presented the most relevant improvement
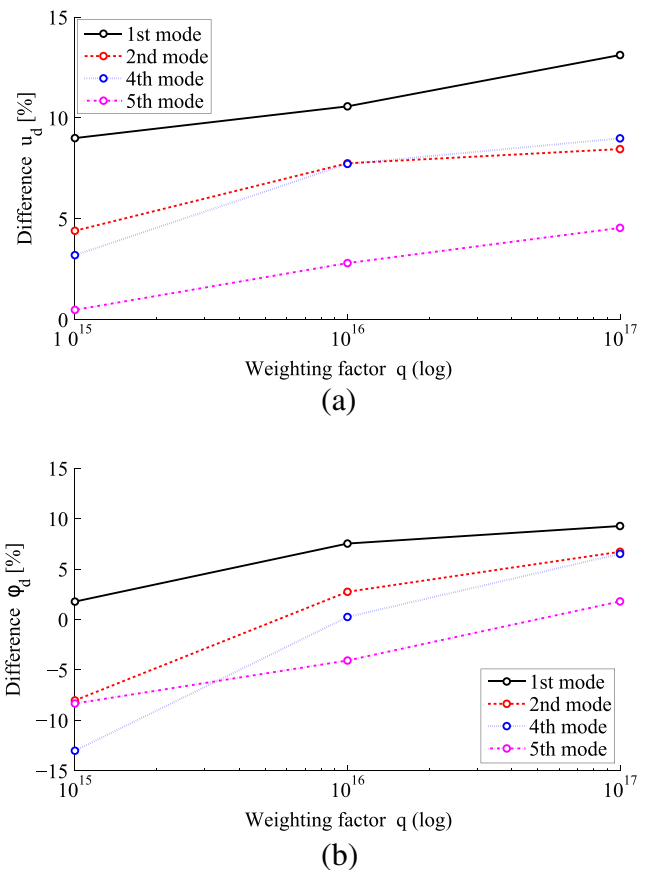
Fig. 15 Difference between designs obtained by uniform and optimal polarization profile: **a** RMS displacement and **b** RMS control voltage, for the cantilever beam example
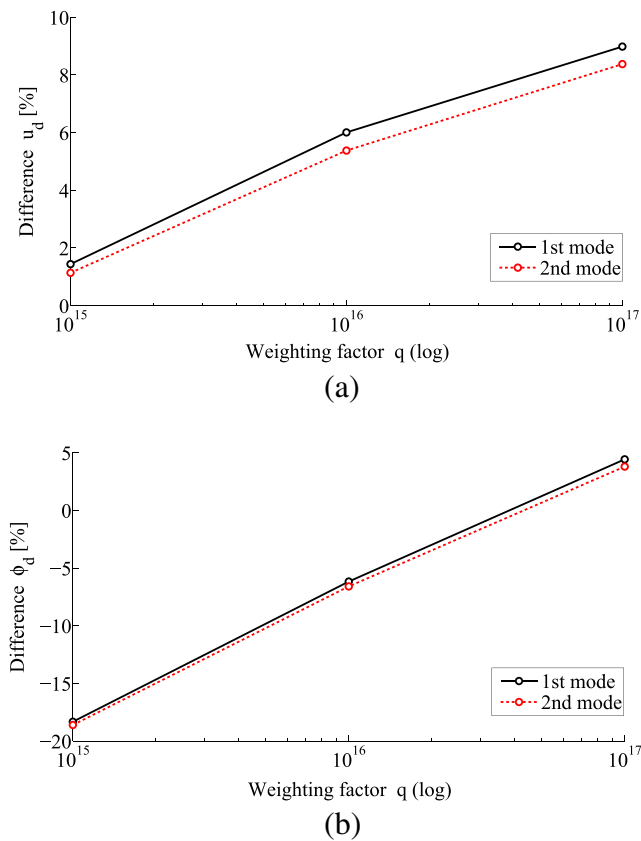
Fig. 16 Difference between designs obtained by uniform and optimal polarization profile: **a** RMS displacement and **b** RMS control voltage, for the fixed beam example

when using the simultaneous approach. For instance, the RMS displacement and control voltage are, respectively, 9.0 and 1.8% lower for case B when using $q = 1 \times 10^{15}$. However, this difference is increased when using higher weighting factors for the control of all vibration modes analyzed here, as it can be seen in Fig. 15.

5 Concluding remarks

In this work, the simultaneous optimization with respect to piezoelectric actuator topology and polarization is investigated. The design of embedded in-plane actuators is carried out by means of a topology optimization problem based on a controllability measure. This is a first approach toward a single formulation that takes into account several aspects for controllability-based designs in topology optimization problems. Actuator designs obtained by the simultaneous approach presented an improvement in control performance for the analyzed cases. Moreover, this approach allows the synthesis of a simple control system with only one input channel which is, therefore, more

suitable for practical applications. However, the polarization profiles presented here also give an insight on possible alternatives to define independent electrodes, where null-polarity areas would be required to separate different electrodes in order to avoid problems as short-circuiting.

References

Allik H, Hughes TJ (1970) Finite element method for piezoelectric vibration. Int J Numer Methods Eng 2(2):151–157

Bartels RH, Stewart GW (1972) Solution of the matrix equation ax + xb = c [f4]. Commun ACM 15(9):820–826

Becker J, Fein O, Maess M, Gaul L (2006) Finite element-based analysis of shunted piezoelectric structures for vibration damping. Comput Struct 84(31):2340–2350

Bendsøe MP, Kikuchi N (1988) Generating optimal topologies in structural design using a homogenization method. Comput Methods Appl Mech Eng 71(2):197–224

Bendsøe MP, Sigmund O (1999) Material interpolation schemes in topology optimization. Arch Appl Mech 69(9):635–654

Bendsøe MP, Sigmund O, Bendsøe MP, Sigmund O (2004) Topology optimization by distribution of isotropic material. Springer, Berlin

Carbonari RC, Silva EC, Nishiwaki S (2007) Optimum placement of piezoelectric material in piezoactuator design. Smart Mater Struct 16(1):207

Chen PJ, Montgomery ST (1980) A macroscopic theory for the existence of the hysteresis and butterfly loops in ferroelectricity. Ferroelectrics 23(1):199–207

Donoso A, Bellido J (2009) Systematic design of distributed piezoelectric modal sensors/actuators for rectangular plates by optimizing the polarization profile. Struct Multidiscip Optim 38(4):347–356

Donoso A, Sigmund O (2016) Topology optimization of piezo modal transducers with null-polarity phases. Struct Multidiscip Optim 53(2):193–203

Gawronski W (2004) Advanced structural dynamics and active control of structures. Springer Science & Business Media, Berlin

Gonçalves JF, Fonseca JSO, Silveira OAA (2016) A controllability-based formulation for the topology optimization of smart structures. Smart Structures and Systems 17(5):773–793

Gonçalves JF, De Leon DM, Perondi EA (2017) Topology optimization of embedded piezoelectric actuators considering control spillover effects. J Sound Vib 388:20–41

Ha Y, Cho S (2006) Design sensitivity analysis and topology optimization of eigenvalue problems for piezoelectric resonators. Smart Mater Struct 15(6):1513

Ha ć A, Liu L (1993) Sensor and actuator location in motion control of flexible structures. J Sound Vib 167(2):239–261

Hammarling S (1991) Numerical solution of the discrete-time, convergent, non-negative definite lyapunov equation. Systems & Control Letters 17(2):137–139

Hughes TJR (2012) The finite element method: linear static and dynamic finite element analysis. Dover Publications, Mineola, New York.

Irschik H (2002) A review on static and dynamic shape control of structures by piezoelectric actuation. Eng Struct 24(1):5–11

Kang Z, Wang R, Tong L (2011) Combined optimization of bi-material structural layout and voltage distribution for in-plane piezoelectric actuation. Comput Methods Appl Mech Eng 200(13):1467–1478

Kim TS, Kim YY (2000) Mac-based mode-tracking in structural topology optimization. Comput Struct 74(3):375–383

Kiyono CY, Silva ECN, Reddy J (2012) Design of laminated piezocomposite shell transducers with arbitrary fiber orientation using topology optimization approach. Int J Numer Methods Eng 90(12):1452–1484

Kögl M, Silva EC (2005) Topology optimization of smart structures: design of piezoelectric plate and shell actuators. Smart Mater Struct 14(2):387

Leleu S, Abou-Kandil H, Bonnassieux Y (2000) Piezoelectric actuators and sensors location for active control of flexible structures. In: Proceedings of the 17th IEEE instrumentation and measurement technology conference, 2000. IMTC 2000, vol 2. IEEE, pp 818–823

Lerch R (1990) Simulation of piezoelectric devices by two-and three-dimensional finite elements. IEEE Trans Ultrason Ferroelectr Freq Control 37(3):233–247

Lund E (2009) Buckling topology optimization of laminated multi-material composite shell structures. Compos Struct 91(2):158–167

Luo Z, Gao W, Song C (2010) Design of multi-phase piezoelectric actuators. J Intell Mater Syst Struct 21(18):1851–1865

Meitzler A, Tiersten H, Warner A, Berlincourt D, Couqin G, Welsh FIII (1988) IEEE Standard on piezoelectricity. ANSI/IEEE, std. 176-1987

Middleton RH, Goodwin GC (1990) Digital control and estimation: a unified approach. Prentice-Hall, Englewood Cliffs, New Jersey

Nakasone PH, Silva ECN (2010) Dynamic design of piezoelectric laminated sensors and actuators using topology optimization. J Intell Mater Syst Struct 21(16):1627–1652

Penzl T (1998) Numerical solution of generalized lyapunov equations. Adv Comput Math 8(1):33–48

Preumont A (2011) Vibration control of active structures: an introduction, vol 179. Springer Science & Business Media, Berlin

Priya S (2007) Advances in energy harvesting using low profile piezoelectric transducers. J Electroceram 19(1):167–184

Rubio WM, Silva EC, Paulino GH (2009) Toward optimal design of piezoelectric transducers based on multifunctional and smoothly graded hybrid material systems. J Intell Mater Syst Struct 20(14):1725–1746

Ruiz D, Bellido J, Donoso A (2016) Design of piezoelectric modal filters by simultaneously optimizing the structure layout and the electrode profile. Struct Multidiscip Optim 53(4):715–730

Seyranian AP, Lund E, Olhoff N (1994) Multiple eigenvalues in structural optimization problems. Struct Multidiscip Optim 8(4):207–227

Silva ECN, Kikuchi N (1999) Design of piezoelectric transducers using topology optimization. Smart Mater Struct 8(3):350

Silveira OAA, Fonseca JSO, Santos IF (2015) Actuator topology design using the controllability gramian. Struct Multidiscip Optim 51(1):145–157

Stolpe M, Svanberg K (2001) An alternative interpolation scheme for minimum compliance topology optimization. Struct Multidiscip Optim 22(2):116–124

Tsai T, Cheng C (2013) Structural design for desired eigenfrequencies and mode shapes using topology optimization. Struct Multidiscip Optim 47(5):673–686

Wein F, Kaltenbacher M, Bänsch E, Leugering G, Schury F (2009) Topology optimization of a piezoelectric-mechanical actuator with single-and multiple-frequency excitation. Int J Appl Electromagn Mech 30(3, 4):201–221

Wu B, Xu Z, Li Z (2007) A note on computing eigenvector derivatives with distinct and repeated eigenvalues. Commun Numer Methods Eng 23(3):241–251

Yin L, Ananthasuresh G (2001) Topology optimization of compliant mechanisms with multiple materials using a peak function material interpolation scheme. Struct Multidiscip Optim 23(1):49–62

Zuo W, Saitou K (2017) Multi-material topology optimization using ordered simp interpolation. Struct Multidiscip Optim 55(2):477–491